Article type: Full paper

Title: Chlorosome-Like Molecular Aggregation of Chlorophyll Derivative on $Ti_3C_2T_x$

MXene Nanosheets for Efficient Noble Metal-Free Photocatalytic Hydrogen Evolution

Yuanlin Li, Xin Chen, Yuliang Sun, Xing Meng, Yohan Dall'Agnese, Gang Chen, Chunxiang

Dall'Agnese, Hangchen Ren, Shin-ichi Sasaki, Hitoshi Tamiaki, Xiao-Feng Wang*

Yuanlin Li and Xin Chen contribute equally to the article

Yuanlin Li, Yuliang Sun, Prof. Xing Meng, Prof. Gang Chen, Dr. Chunxiang Dall'Agnese,
Prof. Xiao-Feng Wang
Key Laboratory of Physics and Technology for Advanced Batteries (Ministry of Education),
College of Physics. Jilin Key Engineering Laboratory of New Energy Materials and
Technologies. Jilin University, Changchun, 130012, P. R. China
*E-mail: Xiao-Feng Wang: xf_wang@jlu.edu.cn
Xin Chen
College of Life Science, Jilin University, Changchun 130012, P. R. China
Dr. Yohan Dall'Agnese
Institute for Materials Discovery, University College London, London WC1E 7JE, United
Kingdom
Hangchen Ren
College of Materials Science and Engineering, Jilin University, Changchun 130012, P. R.
China
Prof. Shin-ichi Sasaki,
Graduate School of Life Sciences, Ritsumeikan University, Kusatsu, Shiga 525-8577.
Nagahama Institute of Bio-Science and Technology, Nagahama, Shiga 526-0829. Japan
Prof. Hitoshi Tamiaki
Graduate School of Life Sciences, Ritsumeikan University, Kusatsu, Shiga 525-8577, Japan

Abstract

Efficient photocatalytic hydrogen evolution reaction (HER) in the visible-to-near infrared region at a low cost remains a challenging issue. This work demonstrates the fabrication of organic-inorganic composites by deposition of supramolecular aggregates of a chlorophyll derivative, namely, zinc methyl 3-devinyl-3-hydroxymethyl-pyropheophorbide a (Chl) on the surface of $Ti_3C_2T_x$ MXene with 2D accordion-like morphology. This composite material was employed as noble metal-free catalyst in photocatalytic HER under the white light illumination, where Chl serves as a small molecule organic semiconductor instead of ordinary inorganic semiconductor and polymer organic semiconductors such as TiO_2 and g-C_3N_4, and $Ti_3C_2T_x$ serves as a co-catalyst. Different composition ratios of Chl/$Ti_3C_2T_x$ were compared for their light-harvesting ability, morphology, charge transfer efficiency, and photocatalytic performance. The best HER performance was found to be as high as 52 ± 5 $\mu mol/h/g_{cat}$ after optimization. Such a large HER activity is attributed to the efficient light harvesting followed by exciton transfer in Chl aggregates and the resultant charge separation at the interface of Chl/$Ti_3C_2T_x$.

1. Introduction

Over exploitation and utilization of traditional fossil fuels are not sustainable owing to many possible negative side effects such as global warming and climate changes.[1-4] Solar energy is clean and abundant, e.g., nearly four million exajoules (4×10^{18} J) of solar energy reaches the earth annually.[1, 5] Conversion of solar energy into chemical energy through photocatalytic decomposition of water to produce hydrogen is one of the suitable approaches to utilize solar energy.[6-10] The main different types of fundamental photocatalytic reactions include (i) semiconductor-based photocatalysis, (ii) dye-sensitized semiconductor-based photocatalysis, (iii) quantum dot-based photocatalysis, (iv) 2D layered materials-based photocatalysts, and (v) plasmonic photocatalysts.[11] Photocatalytic HER are mainly based on

2

inorganic semiconductor and polymer-based organic semiconductors, e.g., in a conventional dye-sensitized semiconductor photocatalytic hydrogen production system, the dye molecules are excited to inject electrons into the conduction band of a semiconductor or polymer (inorganic semiconductor TiO_2 or g-C_3N_4 is usually chosen), then the electrons are quickly captured by the co-catalyst (such as precious metals Pt, Ru and Pd), and finally the electrons combine with H^+ in the water to produce hydrogen.[12-16]

Natural photosynthesis has evolved for billions of years, which converts solar energy into chemical energy based on their light-harvesting antenna systems.[17-18] Chlorosomes are special antenna systems in photosynthetic green bacteria containing self-aggregated chlorophylls for light-harvesting followed by extremely efficient exciton transfer.[19] Simulation of the chlorosomal antenna system is of particular interest for artificial photosynthesis systems owing to the excellent light-harvesting capability of chlorophyll aggregates. The successive long-lifetime charge separated state of chlorophyll molecules can be a key process in solar conversion systems. The intriguing physical properties of chlorosomal antenna systems have stimulated some applications of chlorophyll aggregates in photovoltaic devices such as perovskite solar cells and biosolar cells.[18, 20-22] The special light trapping, electron/excited state migration, and hole back-transfer of chlorophyll aggregates are also the basis for effectively suppressing electron-hole recombination, which is important to improve the efficiency of photocatalytic hydrogen evolution reaction (HER). Therefore, incorporation of chlorophyll aggregates in the photocatalytic HER systems must be of great potential.

MXenes are a new family of 2D nanostructured materials originally reported in 2011.[23] The excellent electrochemical properties of MXenes make them widely applicable for electromagnetic interference shielding,[24-25] photodegradation,[26] photovoltaics,[27-28] electrochemical catalysis,[29] supercapacitors, and lithium ion batteries.[30-32] MXenes are

prepared from MAX phases by etching the A layer (usually Al or Si) with a strong acid solution such as HF or LiF/HCl.[33] The general formula of MXenes is $M_{n+1}X_nT_x$ (n = 1-3), where M represents an early transition metal such as Ti, V, Nb, Ta, or Mo, X is C and/or N, and T_x represents a surface terminating group such as -O, -F and -OH.[32, 34-35] It is worth noting that $Ti_3C_2T_x$ MXene as a co-catalyst has remarkable characteristics such as good hydrophilicity, excellent metallic conductivity, good stability in aqueous solutions, and low cost. Considering the above-mentioned excellent characteristics of $Ti_3C_2T_x$, it has become a very promising co-catalyst material in photocatalysis for HER.[36-38] The photocatalytic activity of TiO_2 P25 for carbon dioxide reduction was enhanced by surface alkalization of titanium carbide MXene as a co-catalyst.[39] The photocatalysts for H_2 and O_2 evolution from water were prepared by in-situ growth strategy of simultaneous oxidation and alkalization of $Ti_3C_2T_x$/TiO_2 nanoflowers.[37] By oxidizing surface groups of g-C_3N_4/$Ti_3C_2T_x$ MXenes composite, the catalytic activity of $Ti_3C_2T_x$ as a co-catalyst was improved for efficient photocatalytic hydrogen evolution.[38] Partially oxidized $Ti_3C_2T_x$ MXene by eosin Y-sensitization was used for high-efficient photocatalytic hydrogen evolution under visible light irradiation.[40] A defect-controlled and sulfur-doped TiO_2 and carbon substrates was synthesized by using 2D transition metal carbide (MXenes) as a template to enhance light absorption and improve charge separation, enabling visible light-driven high-efficient photocatalytic hydrogen production.[41] Other MXenes can also be used, for example, Nb_2O_5/C/Nb_2C (MXene) composites promoted the separation of photogenerated charge carriers and enabled efficient photocatalytic HER.[42] Therefore, MXenes can be used as co-catalysts in photocatalysis and may potentially contribute to decrease the cost of hydrogen production.

In contrast to the traditional system, in this work, inorganic semiconductors were not used, but a chlorophyll-*a* derivative (Chl) was selected as a small molecule organic

semiconductor, for the first time to the best of our knowledge, because of the long-lifetime charge separated state. $Ti_3C_2T_x$ was selected as a co-catalyst to enhance the charge carrier separation. Chl can be excited by visible-to-near infrared light to generate an electron-hole pair, then the electron is directly transferred to the non-noble metal co-catalyst $Ti_3C_2T_x$, which combines with H^+ in aqueous solution to generate hydrogen gas. The effect of $Chl/Ti_3C_2T_x$ ratio on the hydrogen production under the above light irradiation was studied. Electrochemical impedance spectroscopy (EIS) and transient photocurrent (TPC) response tests showed that the HER rates of these composites were related to the kinetics between Chl and $Ti_3C_2T_x$. Different ratios of $Chl/Ti_3C_2T_x$ significantly affected the charge transfer and recombination, thus affected the photocatalytic efficiency.

2 Results and discussion

2.1 Structures and morphology

Figure 1a shows a schematic representation of the preparation method. $Ti_3C_2T_x$ is prepared by etching the Al layer of Ti_3AlC_2 powder with HF.[43] During the HF etching process, the -OH, -F and -O surface terminating groups are spontaneously formed on the surface of $Ti_3C_2T_x$, resulting in enhanced hydrophilicity of $Ti_3C_2T_x$.[44] Figure 1b shows XRD patterns of the raw materials and composites studied herein. The (002) and (004) peaks move toward low angles and the strongest MAX phase peak at 39 degree disappeared, indicating that the Al layer is removed from Ti_3AlC_2. The XRD pattern of Chl shows three typical peaks 6.2°, 13.9°, and 25.2°. The XRD pattern of the composite only shows the characteristic pattern of $Ti_3C_2T_x$, and there are not the three typical peaks of Chl. This is mainly due to the low Chl mass ratio.

Figure 1c shows the FT-IR spectra of these raw materials and composites. As previously reported, the two signals at 1390 and 1650 cm^{-1} can be attributed to O-H and C=O on $Ti_3C_2T_x$.[45] The three small peaks between 2750 and 3000 cm^{-1} belong to -CH_2 and -CH_3 of

Chl. Moreover, the strengths of the vibration peaks in the composite increase with the increase of the concentration of Chl.
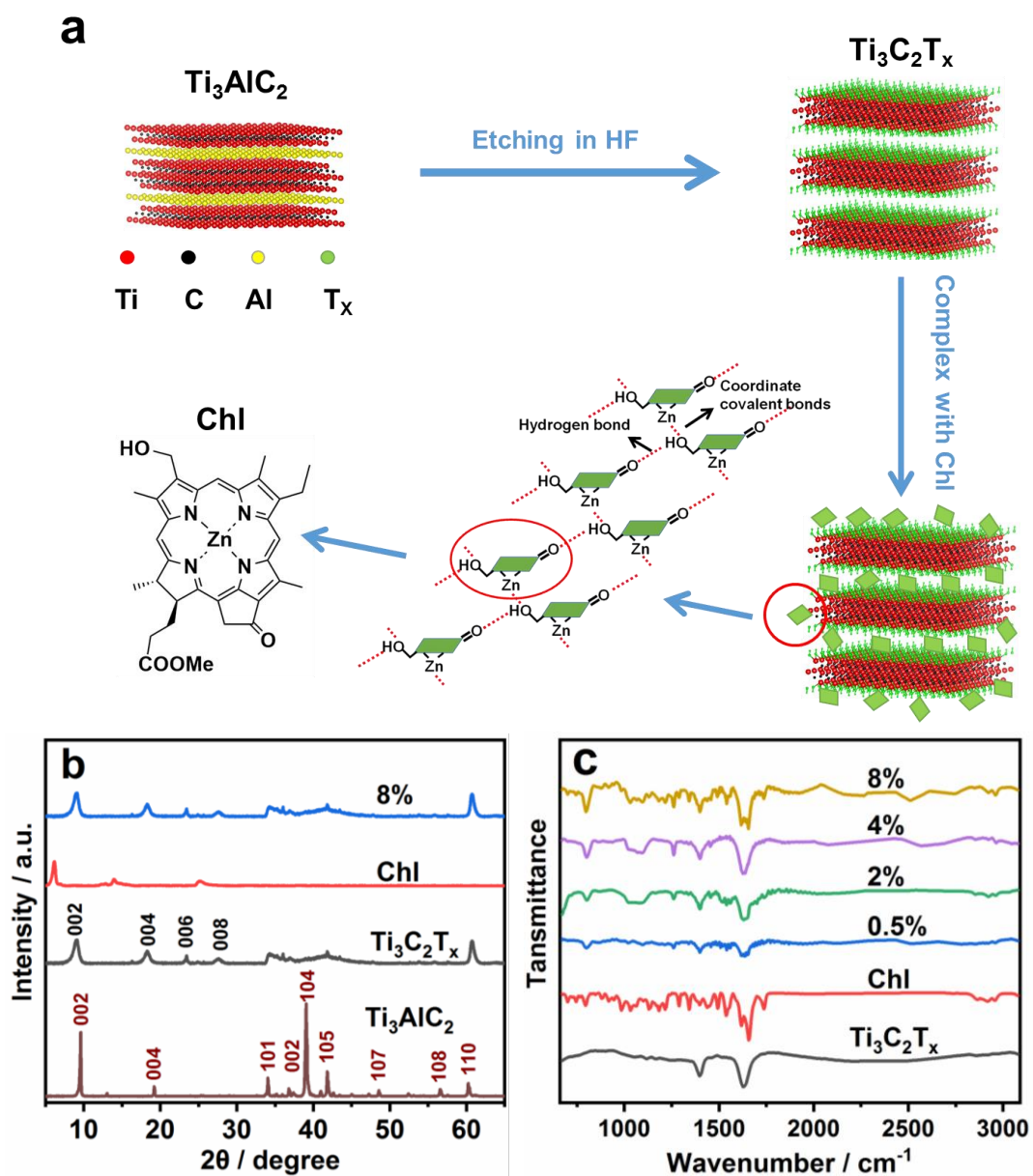

Figure 1. (a) Schematic diagram of the preparation process of Chl/Ti$_3$C$_2$T$_x$ composites, (b) XRD patterns of the three raw materials and the composites, and (c) FTIR spectra of the two raw materials and the composites.

Figure 2 shows the morphology of the $Ti_3C_2T_x$, Chl, and composites by SEM. As shown in Figure 2a, a typical 2D nanosheet accordion-like structure can be clearly observed in the HF-etched $Ti_3C_2T_x$. In Figure 2b, it can be seen that Chl is a kind of 2D material with a layered structure. When Chl and $Ti_3C_2T_x$ are mixed in different proportions, only the typical 2D nanosheet stack structure of $Ti_3C_2T_x$ is observed, and no other significant changes are observed, as shown in Figure 2c-f. Because Chl is a small molecule aggregate, not a macromolecular aggregate. The amount of small molecule aggregate on $Ti_3C_2T_x$ is also very low. Though Figure 2b shows the aggregate of pure Chl, it is too small to see after deposited on surface of $Ti_3C_2T_x$. So it is difficult to observe Chl with $Ti_3C_2T_x$ in SEM images.
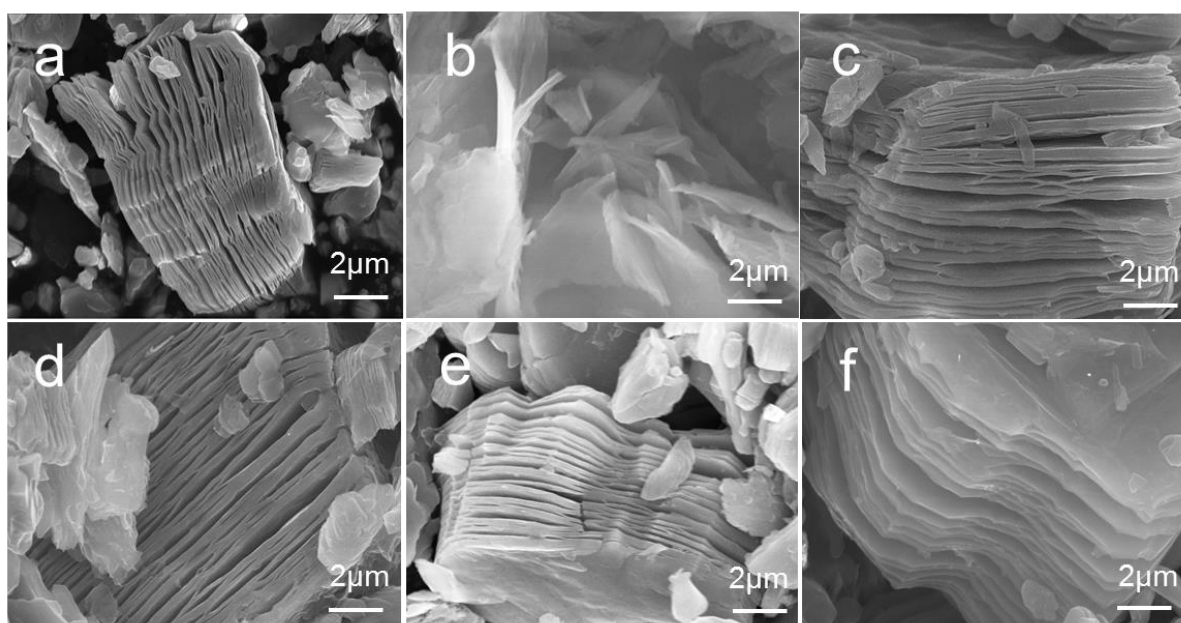
Figure 2. SEM images of (a) $Ti_3C_2T_x$, (b) Chl, (c) $Ti_3C_2T_x$ with 0.5% Chl, (d) $Ti_3C_2T_x$ with 2% Chl, (e) $Ti_3C_2T_x$ with 4% Chl, and (f) $Ti_3C_2T_x$ with 8% Chl.

Table 1 lists the composites elements ratios of different samples obtained by EDS. The composite ratio of Zn and Ti increases as the ratio of Chl increases (Figure S1). By calculation, the actual composite ratio of Chl and $Ti_3C_2T_x$ samples also increases with the increase of Chl. Moreover, the actual composite ratio of the sample is larger than the sample

designed ratio, which is due to the inhomogeneous distribution of Chl on 2D $Ti_3C_2T_x$ layer, specifically, most of the Chl is distributed on the surface of $Ti_3C_2T_x$.

Table 1. The EDS surveys of two raw materials and different hybrids.

Sample	$Ti_3C_2T_x$	Chl	0.5%	2%	4%	8%
Calculated mass ratio of Chl to $Ti_3C_2T_x$ (EDS)	0	100%	0.81%	2.46%	6.6%	9.9%

2.2 Electronic absorption

Figure 3 shows electronic absorption spectra of the samples in water. Electronic absorption spectrum is a widely used method for studying the light absorption in semiconductor-based photocatalysts. As previously reported, $Ti_3C_2T_x$ has no significant absorption peak due to its metallic properties.[46] Pure Chl and Chl/$Ti_3C_2T_x$ composites show the absorption band around the wavelength of 750 nm, reflecting the band gap of Chl.[47] Therefore, the band gap of the composite material does not change obviously. In view of this, light absorption is negligible in discussing the HER performance of these Chl/$Ti_3C_2T_x$ composites. Since the sample are dispersed in water, the baseline of the electronic absorption spectra is fluctuated (see also Figure S2). Because the sample is insoluble in water, the sample is dispersed in water instead of dissolved in water, which may cause little difference in the intensity of electronic absorption.
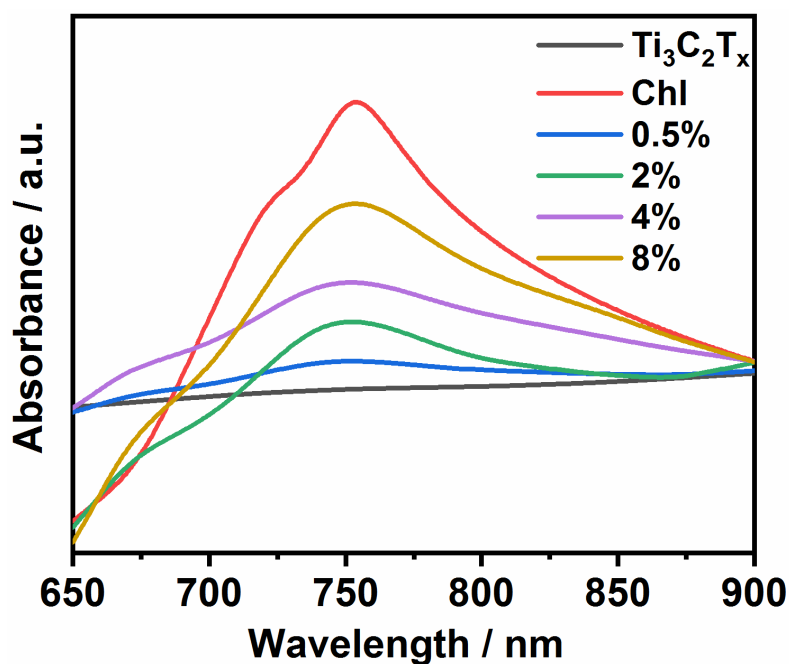
Figure 3. Electronic absorption spectra of all as-prepared samples in water.

2.3 Photocatalytic performance

These composites are tested as photocatalysts for water splitting. The HER performances of 3 mg of $Ti_3C_2T_x$ with a different amount of Chl are shown in Figure 4a. The photocatalytic hydrogen production of the $Chl/Ti_3C_2T_x$ composites are evaluated by visible-to-near infrared light ($\lambda > 400$ nm). As the Chl content increases from 0.5% to 2%, the hydrogen production increases. The best performance was achieved for the $Chl/Ti_3C_2T_x$ composite containing 2% of Chl, with the hydrogen production reaching as high as 20 ± 2 µmol/h/g. This is because with the increase of Chl adsorption, more photogenerated electrons are transferred from Chl to $Ti_3C_2T_x$. When the Chl amount increases more than 2%, less excited electrons can be transferred to $Ti_3C_2T_x$ in time. Therefore, the recombination of electrons and holes generated by Chl upon light absorption increases, resulting in a decrease in hydrogen production.[48]
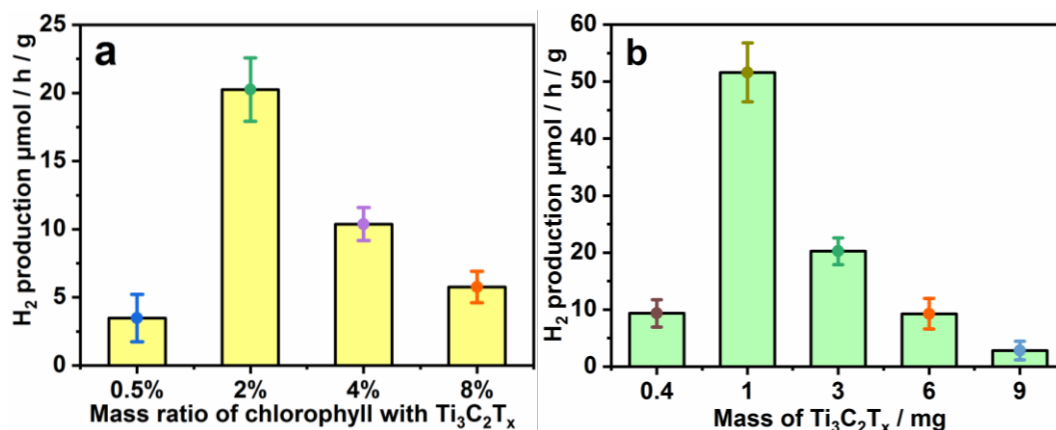
9

Figure 4. The hydrogen production of (a) 3 mg $Ti_3C_2T_x$ with Chl at different mass ratio and (b) 60 μg Chl with different $Ti_3C_2T_x$ mass.

Figure 4b compares the HER results of composites containing 60 μg Chl and different mass of $Ti_3C_2T_x$. When the mass of $Ti_3C_2T_x$ is 1 mg, the hydrogen production reaches a maximum of 52 ± 5 μmol/h/g. As $Ti_3C_2T_x$ increases from 0.4 mg to 1 mg, hydrogen production increases. This is because photoelectrons are more easily transferred from Chl to $Ti_3C_2T_x$ as $Ti_3C_2T_x$ increases and more active sites for HER. When $Ti_3C_2T_x$ is increased more than 1 mg, $Ti_3C_2T_x$ affects the light absorption of Chl and the active sites decrease, resulting in a decrease in hydrogen production.

We also discussed the HER in another calculation method. In Figure S3, the production of hydrogen was calculated by the Chl mass. The best hydrogen production reaches 1010 ± 110 μmol/h/g_{Chl}. We also evaluated the HER at λ > 600 nm as shown in Figure S4. Comparing with the activity (λ > 400 nm), the performance (λ > 600 nm) was suppressed by the less light absorption, but the red-to-near infrared light was useful for the HER due to the Q_y band (see Figure 3).

2.4 Photoelectrochemical measurement

Figure 5 shows the EIS and TPC response tests to further study the improvement of carrier separation efficiency.[49] The EIS Nyquist plot can be fitted to the equivalent circuit shown in Figure 5a (inset), where R_1 is the electrolyte solution resistance and R_2 is the

interface charge transfer resistance between electrode and electrolyte, respectively, and CPE and W_0 are the constant phase element and the Warburg impedance, respectively.[42] The smaller semi-circle radius on the EIS Nyquist diagram means a lower electron transfer resistance on the electrode surface. This usually leads to more efficient separation of photoelectron-hole pairs and faster interface charge transfer. As shown in Figure 5a, the radius of the semi-circle of the 2% Chl/Ti$_3$C$_2$T$_x$ composite is much smaller than those of the others. Based on the fitting model, the fitting data for the samples are summarized in Table S1, in which the R_2 value of the 2% Chl/Ti$_3$C$_2$T$_x$ composite is the smallest of these samples. This indicates a high electron-hole pair separation efficiency. Initially, as Chl was continuously adsorbed on the surface of Ti$_3$C$_2$T$_x$, excited state electrons were continuously transferred to Ti$_3$C$_2$T$_x$. However, as the Chl content is greater than 2%, the interface transfer resistance increases due to too much Chl, making it difficult to transfer excited electrons to Ti$_3$C$_2$T$_x$. Therefore, the amount of hydrogen produced decreases.
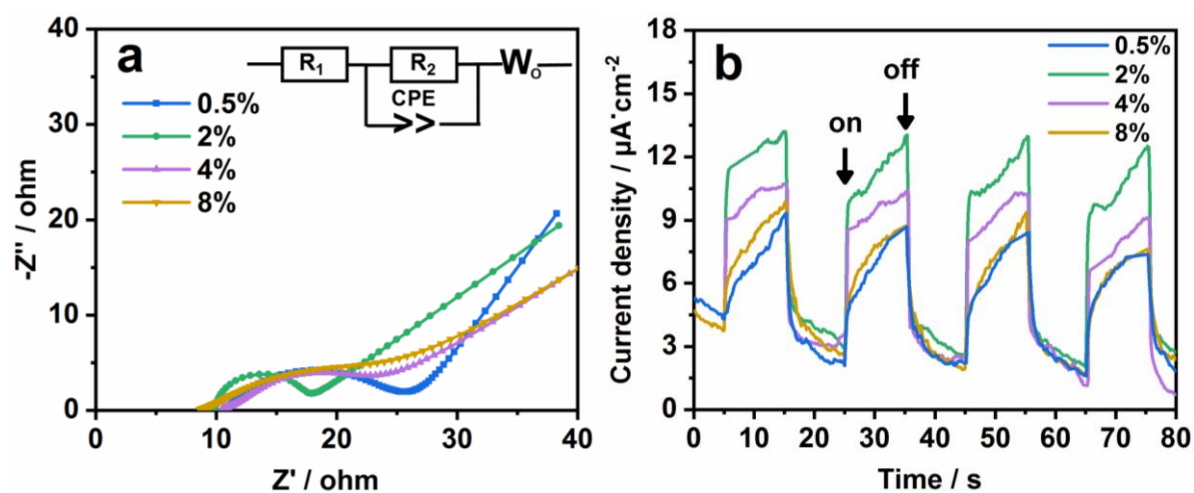

Figure 5. (a) EIS Nyquist plots and (b) transient photocurrent responses of the hybrids.

Figure 5b compares the photocurrent-time (I-t) curves for different samples. It can be seen that all samples show an immediate rise of TPC response when illuminated by light.[46] 2% Chl/Ti$_3$C$_2$T$_x$ composites show higher photocurrent strength than other composites. This means that 2% Chl/Ti$_3$C$_2$T$_x$ composite can achieve higher photogenerated carrier separation

and transfer efficiency. EIS and TPC results are consistent with each other. It is confirmed that the 2% $Chl/Ti_3C_2T_x$ composite has an optimal charge transfer rate compared to other composites, which explains its improved photocatalytic activity.

2.5 Photocatalytic mechanism

Figure 6 shows a hypothetic schematic diagram of the $Chl/Ti_3C_2T_x$ composite for HER. After Chl aggregates are excited by visible-to-near infrared light, the excited state is transferred inside a Chl aggregate. When the excitonic state is reached at the $Ti_3C_2T_x$ contact surface, charge separation occurs. After the photogenerated electron transfer to $Ti_3C_2T_x$, the electrons combine with H^+ in an aqueous AA solution to generate hydrogen gas. The generated hole is returned to the other end of Chl self-aggregate to react with AA (a sacrificial agent). Such expansion of the distance between electron and hole will make the electron-hole pair separation more effective and suppress their recombination, resulting in improved photocatalytic activity with these composites.[50] The holes of Chl are reduced by the electron donor AA, so that the photocatalyst Chl is completely regenerated.
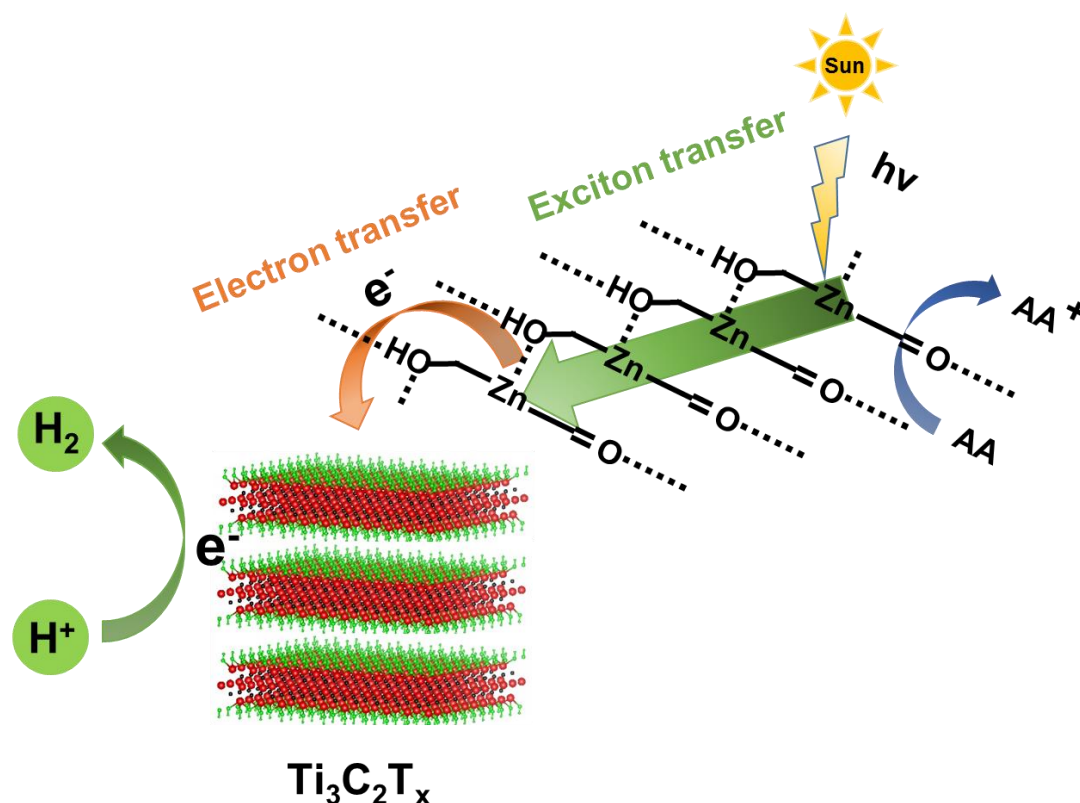
Figure 6. Schematic diagram of hydrogen production for Chl/Ti$_3$C$_2$T$_x$ composite under visible light irradiation.

3. Conclusion

Due to the special light capture and excitonic state transfer of Chl aggregates, and the excellent metallic conductivity of the two-dimensional titanium carbide MXene Ti$_3$C$_2$T$_x$, in this paper, the HER was carried out using composites of Chl and Ti$_3$C$_2$T$_x$. By changing the ratios of Chl to Ti$_3$C$_2$T$_x$, the separation efficiency of electron-hole pairs of the composites is improved and thus the photocatalytic activity is optimized. The best HER performance, as high as 52±5 µmol/h/g, is obtained at a ratio of ≈2% (60 µg) Chl to (1 mg) Ti$_3$C$_2$T$_x$. Compared to other MXenes-based photocatalysts previously reported, this Chl/Ti$_3$C$_2$T$_x$ composite has the long charge separated state and shows better artificial simulated photosynthesis. This work leads to a new understanding of hydrogen evolution based on small molecule organic semiconductors without noble metal catalysts, and provides infinite possibilities to produce hydrogen at a low cost.

4. Experimental section

4.1 Synthesis of Chl and Ti$_3$C$_2$T$_x$ MXenes

Chl were prepared as previously reported.[51] Ti$_3$C$_2$T$_x$ MXenes are obtained by etching Ti$_3$AlC$_2$ (Forsman, 98%) in 49% HF. 20 mL of 49% HF was stirred at 300 rpm/min, and 2 g Ti$_3$AlC$_2$ were slowly added at room temperature for 24 hours. After that, the mixed solutions were washed and centrifuged with deionized water several times until neutral pH was reached, then the sediment was collected after discarding the supernatant. Finally, Ti$_3$C$_2$T$_x$ MXenes was dried in a vacuum oven at 50 °C for 12 hours.

4.2 Preparation of Chl/Ti$_3$C$_2$T$_x$ composites

3 mg Ti$_3$C$_2$T$_x$ and a certain amount of Chl were dissolved in tetrahydrofuran (THF). The mass ratios between Chl and Ti$_3$C$_2$T$_x$ were 0.5% (15 µg), 2% (60 µg), 4% (120 µg), or 8%

(240 μg). The mixture was stirred at room temperature for 10 hours until dry. 60 μg of Chl was weighed, and then 0.4 mg ($\approx$ 15%), 1 mg ($\approx$ 6%), 3 mg ($\approx$ 2%), 6 mg ($\approx$ 1%), and 9 mg ($\approx$ 0.66%) of $Ti_3C_2T_x$ were weighed. 60 μg Chl and $Ti_3C_2T_x$ were dissolved in THF. The mixture was stirred at room temperature for 10 hours until dry.

4.3 Characterization

To characterize Chl, $Ti_3C_2T_x$, and the composites, an X-ray diffractometer (XRD, DX-2700B) was operated at 40 kV and 200 mA with Cu Kα radiation (λ=0.15406 nm). Scanning electron microscopy (SEM, SU8000) was used to observe the morphology of the samples. Fourier transform infrared spectroscopy (FTIR, Vertex70, Bruker, Germany) was used in a range of 600 to 3100 cm^{-1} to record the spectra of the samples. Energy-dispersive X-ray spectroscopy (EDS, Magellan400) mapping was measured to investigate the distribution of element. Electronic absorption spectra (UV-vis, UV-1900) were measured for the absorption of samples under UV-vis light.

4.4 Photocatalytic activity measurements

Photocatalytic H_2 evolution was measured under a 350 W xenon lamp (AHD 350, Shenzhen Anhongda Opto Technology Co. Ltd., China). The light intensity of the 350W Xenon lamp was 80 mW cm^{-2}. A 6 mL photoreactor and a cut-off filter (usually λ > 400 nm and specifically λ > 600 nm) were used. 3 mg of Chl/$Ti_3C_2T_x$ photocatalyst composite was added in 3 mL of 55 mM aqueous ascorbic acid (AA) solution. The mixture was sonicated for 5 min before light irradiation to fully disperse the composite. Argon was purged to remove oxygen in the solution and the reactor for 10 min. The reactants were continuously stirred under the light irradiation. The hydrogen production was measured by a gas chromatograph (SP-3420A, Beijing Beifen-Ruili Analytical Instrument Co. Ltd) with a thermal conductivity detector: the average values were obtained by five independent experiments. The carrier gas was argon and the column contained 5A molecular sieves.

4.5 Photoelectrochemical activity test

EIS measurements in the range of 0.1 Hz to 100 kHz were carried out with an electrochemical workstation (Bio-Logic SAS) in a standard three-electrode system. Chl/$Ti_3C_2T_x$ composite on fluorine-doped tin oxide (FTO) glass was used as the working electrode, Ag/AgCl was used as the reference electrode and Pt plate was used as the counter electrode. The electrolyte was 0.5 M Na_2SO_4 aqueous solution containing 2 g/L AA. TPC response was measured in the same three-electrode system. A 350 W xenon lamp with a cut-off filter ($\lambda > 400$ nm) was used as the light source. The working electrode was prepared by ultrasonically dispersing 10 mg of the Chl/$Ti_3C_2T_x$ composite in a mixture of deionized water (250 μL), ethanol (250 μL) and Nafion solution (20 μL, Sigma-Aldrich, 5 wt%) for 5 min, then 20 μL of the dispersion was drop coated at room temperature onto an 2 cm^2 FTO square substrate.[42] All measurements were conducted at room temperature.

4.6 Electronic absorption activity test

Take six 10 ml containers and add $Ti_3C_2T_x$, Chl, $Ti_3C_2T_x$ with 0.5% Chl, $Ti_3C_2T_x$ with 2% Chl, $Ti_3C_2T_x$ with 4% Chl, and $Ti_3C_2T_x$ with 8% Chl. Add 3 mg of sample and 3 ml of water to the container. And stir for 10 minutes. Then sonicate for 10 minutes to fully disperse the sample.

Supporting Information

Supporting Information is available from the Wiley Online Library or from the author.

Conflicts of interest

There are no conflicts to declare.

References

[1] J. Ran, J. Zhang, J. Yu, M. Jaroniec, S. Z. Qiao, *Chem. Soc. Rev.* **2014**, *43*, 7787.

[2] A. Kudo, Y. Miseki, *Chem. Soc. Rev.* **2009**, *38*, 253.

[3] X. Lu, S. Xie, H. Yang, Y. Tong, H. Ji, *Chem. Soc. Rev.* **2014**, *43*, 7581.

[4] Y. Tachibana, L. Vayssieres, J. R. Durrant, *Nat. Photonics.* **2012**, *6*, 511.

[5] E. Kabir, P. Kumar, S. Kumar, A. A. Adelodun, K.-H. Kim, *Renew. Sustain. Energy. Rev.* **2018**, *82*, 894.

[6] Y. Qu, X. Duan, *Chem. Soc. Rev.* **2013**, *42*, 2568.

[7] P. Du, R. Eisenberg, *Energy Environ. Sci.* **2012**, *5*, 6012.

[8] J. C. Colmenares, R. Luque, *Chem. Soc. Rev.* **2014**, *43*, 765.

[9] C. Peng, H. Wang, H. Yu, F. Peng, *Mater. Res. Bull.* **2017**, *89*, 16.

[10] H. Wang, R. Peng, Z. D. Hood, M. Naguib, S. P. Adhikari, Z. Wu, *ChemSusChem.* **2016**, *9*, 1490.

[11] X. Yang, D. Wang, *ACS Appl. Energy. Mater.* **2018**, *1*, 6657.

[12] K. Takanabe, K. Kamata, X. Wang, M. Antonietti, J. Kubota, K. Domen, *Phys. Chem. Chem. Phys.* **2010**, *12*, 13020.

[13] X. Zhang, U. Veikko, J. Mao, P. Cai, T. Peng, *Chem. Eur. J.*, **2012**, *18*, 12103.

[14] T. Swetha, I. Mondal, K. Bhanuprakash, U. Pal, S. P. Singh, *ACS Appl. Mater. Interfaces.* **2015**, *7*, 19635.

[15] W. Kim, T. Tachikawa, T. Majima, C. Li, H.-J. Kim, W. Choi, *Energy Environ. Sci.* **2010**, *3*, 1789.

[16] Y.-J. Yuan, J.-R. Tu, Z.-J. Ye, H.-W. Lu, Z.-G. Ji, B. Hu, Y.-H. Li, D.-P. Cao, Z.-T. Yu, Z.-G. Zou, *Dyes & Pigments.* **2015**, *123*, 285.

[17] Y. Sun, X.-F. Wang, G. Chen, C.-H. Zhan, O. Kitao, H. Tamiaki, S.-i. Sasaki, *Int. J. Hydrog. Energy.* **2017**, *42*, 15731.

[18] M. Li, Y. Li, S. I. Sasaki, J. Song, C. Wang, H. Tamiaki, W. Tian, G. Chen, T. Miyasaka, X. F. Wang, *ChemSusChem.* **2016**, *9*, 2862.

[19] J. Harada, Y. Shibata, M. Teramura, T. Mizoguchi, Y. Kinoshita, K. Yamamoto, H. Tamiaki, *ChemPhotoChem.* **2018**, *2*, 190.

[20] M. Li, S.-i. Sasaki, Y. Sanehira, T. Miyasaka, H. Tamiaki, T. Ikeuchi, G. Chen, X.-F. Wang, *J. Photochem. Photobiol. A: Chem.* **2018**, *353*, 639.

[21] S. Duan, C. Dall'Agnese, G. Chen, X.-F. Wang, H. Tamiaki, Y. Yamamoto, T. Ikeuchi, S.-i. Sasaki, *ACS Energy. Lett.* **2018**, *3*, 1708.

[22] W. Zhao, C. Dall'Agnese, S. Duan, Y. Sanehira, Y. Wei, H. Tamiaki, S.-i. Sasaki, X.-F. Wang, *ACS Energy. Lett.* **2019**, *4*, 384.

[23] M. Naguib, M. Kurtoglu, V. Presser, J. Lu, J. Niu, M. Heon, L. Hultman, Y. Gogotsi, M. W. Barsoum, *Adv. Mater.* **2011**, *23*, 4248.

[24] X. Li, X. Yin, M. Han, C. Song, H. Xu, Z. Hou, L. Zhang, L. Cheng, *J. Mater. Chem. C* **2017**, *5*, 4068.

[25] M. Han, X. Yin, H. Wu, Z. Hou, C. Song, X. Li, L. Zhang, L. Cheng, *ACS Appl. Mater. Interfaces.* **2016**, *8*, 21011.

[26] H. Huang, Y. Song, N. Li, D. Chen, Q. Xu, H. Li, J. He, J. Lu, *Appl. Catal. B: Environ.* **2019**, *251*, 154.

[27] L. Yang, C. Dall'Agnese, Y. Dall'Agnese, G. Chen, Y. Gao, Y. Sanehira, A. K. Jena, X. F. Wang, Y. Gogotsi, T. Miyasaka, *Adv. Funct. Mater.* **2019**, *29*, 1905694.

[28] A. Agresti, A. Pazniak, S. Pescetelli, A. Di Vito, D. Rossi, A. Pecchia, M. Auf der Maur, A. Liedl, R. Larciprete, D. V. Kuznetsov, D. Saranin, A. Di Carlo, *Nat. Mater.* **2019**, *18*, 1228.

[29] Z. W. Seh, K. D. Fredrickson, B. Anasori, J. Kibsgaard, A. L. Strickler, M. R. Lukatskaya, Y. Gogotsi, T. F. Jaramillo, A. Vojvodic, *ACS Energy. Lett.* **2016**, *1*, 589.

[30] Z. Pan, F. Cao, X. Hu, X. Ji, *J. Mater. Chem. A* **2019**, *7*, 8984.

[31] S. Sun, Z. Xie, Y. Yan, S. Wu, *Chem. Eng. J.* **2019**, *366*, 460.

[32] B. Anasori, M. R. Lukatskaya, Y. Gogotsi, *Nat. Rev. Mater.* **2017**, *2*, 16098.

[33] M. Alhabeb, K. Maleski, B. Anasori, P. Lelyukh, L. Clark, S. Sin, Y. Gogotsi, *Chem. Mater.* **2017**, *29*, 7633.

[34] H. Zhang, M. Li, J. Cao, Q. Tang, P. Kang, C. Zhu, M. Ma, *Ceram. Int.* **2018**, *44*, 19958.

[35] M. Naguib, V. N. Mochalin, M. W. Barsoum, Y. Gogotsi, *Adv. Mater.* **2014**, *26*, 992.

[36] K. Xiong, P. Wang, G. Yang, Z. Liu, H. Zhang, S. Jin, X. Xu, *Sci. Rep.* **2017**, *7*, 15095.

[37] Y. Li, X. Deng, J. Tian, Z. Liang, H. Cui, *Appl. Mater.* **2018**, *13*, 217.

[38] Y. Sun, D. Jin, Y. Sun, X. Meng, Y. Gao, Y. Dall'Agnese, G. Chen, X.-F. Wang, *J. Mater. Chem. A,* **2018**, *6*, 9124.

[39] M. Ye, X. Wang, E. Liu, J. Ye, D. Wang, *ChemSusChem.* **2018**, *11*, 1606.

[40] Y. Sun, Y. Sun, X. Meng, Y. Gao, Y. Dall'Agnese, G. Chen, C. Dall'Agnese, X.-F. Wang, *Catal. Sci. Tech.* **2019**, *9*, 310.

[41] W. Yuan, L. Cheng, Y. An, S. Lv, H. Wu, X. Fan, Y. Zhang, X. Guo, J. Tang, *Adv. Sci.* **2018**, *5*, 170.

[42] T. Su, R. Peng, Z. D. Hood, M. Naguib, I. N. Ivanov, J. K. Keum, Z. Qin, Z. Guo, Z. Wu, *ChemSusChem.* **2018**, *11*, 688.

[43] Z. Guo, J. Zhou, L. Zhu, Z. Sun, *J. Mater. Chem. A* **2016**, *4*, 11446.

[44] M. A. Hope, A. C. Forse, K. J. Griffith, M. R. Lukatskaya, M. Ghidiu, Y. Gogotsi, C. P. Grey, *Phys Chem. Chem. Phys.* **2016**, *18*, 5099.

[45]   Q. Xue, H. Zhang, M. Zhu, Z. Pei, H. Li, Z. Wang, Y. Huang, Y. Huang, Q. Deng, J. Zhou, S. Du, Q. Huang, C. Zhi, *Adv. Mater.* **2017**, *29*, 201604847.

[46]   J. Ran, G. Gao, F. T. Li, T. Y. Ma, A. Du, S. Z. Qiao, *Nat. Commun.* **2017**, *8*, 13907.

[47]   Y. Lu, M. Yao, A. Zhou, Q. Hu, L. Wang, *J. Nanomater.* **2017**, *2017*, 1.

[48]   M. Shao, Y. Shao, J. Chai, Y. Qu, M. Yang, Z. Wang, M. Yang, W. F. Ip, C. T. Kwok, X. Shi, Z. Lu, S. Wang, X. Wang, H. Pan, *J. Mater. Chem. A.* **2017**, *5*, 16748.

[49]   X. An, W. Wang, J. Wang, H. Duan, J. Shi, X. Yu, *Phys. Chem. Chem. Phys.* **2018**, *20*, 11405.

[50]   X. Xie, N. Zhang, Z.-R. Tang, M. Anpo, Y.-J. Xu, *Appl. Catal. B: Environ.* 2018, *237*, 43.

[51]   H. Tamiaki, M. Amakawa, Y. Shimono, R. Tanikaga, A. R. Hotzwarth, K. Schaffner, *Photochem. Photobiol.* 1996, *63*, 92.